

Recipe for observing immediate entanglement death-birth transition through Bell states with environmental Heisenberg exchange

Son-Hsien Chen (陳松賢)^{1,*} Seng Ghee Tan,² and Che-Chun Huang^{3,4}

¹*Department of Applied Physics and Chemistry, University of Taipei, Taipei 10048, Taiwan*

²*Department of Optoelectric Physics, Chinese Culture University, Taipei 11114, Taiwan*

³*Department of Advanced Metrology, Taiwan Semiconductor Manufacturing Company Limited, Hsinchu 300091, Taiwan*

⁴*Department of Physics, National Taiwan University, Taipei 10617, Taiwan*

(Dated: October 6, 2024)

Environment is known to play a dual role in both extinguishing and establishing entanglement, leading to entanglement sudden death (ESD) and entanglement sudden birth (ESB). In this paper, we propose a recipe for the initial states of two qubits to undergo ESD, ESB, or transition of finite duration (TFD) between them. While this recipe is generic, a spin-star model coupled to the environment via Heisenberg exchange is chosen for illustration. Utilizing the Bell states, we introduce the entanglement switch parameter (ESP), whose sign indicates whether the qubit bipartite entanglement is switched on or off. The classical (quantum) weighting of the Bell states encodes the ESP for initial mixed (pure) states. When more than two Bell states are adopted, the ESP permits states to penetrate through the entanglement-unentanglement boundary. In this case, the penetrability of a small ESP ensures the immediate occurrence of ESD or ESB and indicates the TFD if the local time-even symmetry in the entanglement monotone is also satisfied. When no more than two Bell states are employed, the penetrability is lost, and TFD is only identified in some mixed states but not in pure states. For pure states, the environmental quantum degrees of freedom are associated with the number of Bell states. Thanks to the simplicity of this model, analytic results are provided. We also analyze the symmetries that can convert or alter ESD into ESB, and vice versa. The recipe enhances the controllability of entanglement dynamics and facilitates entanglement engineering.

I. INTRODUCTION

Quantum entanglement [1], which characterizes constituent subsystems that are not tensor-product separable, plays a crucial role in quantum technologies [2], including gravitational wave detection [3, 4], quantum cryptography [5–8], and quantum computation [1, 9–14]. Once established, this quantum correlation can persist even when each subsystem is isolated [15]. On the other hand, in open systems where an interacting environment or medium is introduced to the subsystems, the environment triggers decoherence [16] and can play dramatically different roles—inducing entanglement, suppressing it, or even both.

In the case of suppression, interactions with environment can lead to the disappearance of entanglement. However, unlike typical subsystem decoherence process, where coherence dies out asymptotically [17, 18], the alteration from entanglement to unentanglement can occur suddenly for both mixed and pure initial states [19]. For instance, a pioneering study predicted that two entangled atoms, each with two levels and encapsulated in their cavities, can abruptly become fully unentangled after a finite time due to vacuum fluctuations via spontaneous emissions [20]. This phenomenon, known as entanglement sudden death (ESD) [21–24], was later confirmed experimentally using optical setups [25]. Furthermore, it was recently pointed out [15] that ESD is more likely to

arise in the minimal set of bipartite entanglement, consisting of a pair ($N = 2$) of qubits ($d = 2$), but less likely in the entanglement beyond the minimal set, $N > 2$ or $d > 2$. Here, d indicates the qudit dimension, i.e., the number of eigenstates (or energy levels) a subsystem can occupy, and N specifies the number of qudits. Indeed, most existing research identifying ESD pertains to the minimal set [19, 20, 24–30]. The ESD has also been experimentally observed in solid-state systems [29]. A few techniques have been developed to postpone ESD [31–34]. By adjusting the initial states within certain amount of entanglement, excitation, and purity, the ESD can be avoided [32].

It is also well known that the environment can provoke subsystem entanglement [35–43]. During measurement, the environment interacts with subsystems, allowing quantum information to be sensed and extracted; even random interactions can establish, preserve, and extend entanglement [44], as well as alter the spatial scaling law [45–47] of the saturated entanglement. In addition, entanglement mechanism has garnered significant attention and is considered essential in the field of spintronics [48]. In particular, recent developments employing inelastic neutron scattering [49–51] and X-ray scattering [52–54] have enabled the detection of entanglement in spintronics devices. Notably, two distant macroscopic ferromagnets can become entangled through spin exchange mediated by electrons [55], disrupting the conservation of local ferromagnet magnetization. This conservation can be process-dependent, influenced by whether the dynamics is non-Markovian or Markovian [56]. The resulting non-conservation of magnetization limits the

* sonhsien@utapei.edu.tw

applicability of classical spin equations of motion, such as the Landau-Lifshitz-Gilbert equation. The mediated entanglement is also realized in a similar microscopic model known as the spin-star network [57], where all subsystem spins interact exclusively with a central environmental spin through Heisenberg exchange. In this model, the entanglement mediating capability of the central spin depends on the total number of subsystem spins. Moreover, in the minimal set of two qubits [58–60], not only has ESD been identified, but the revival of entanglement, conventionally termed entanglement sudden birth (ESB), has also been discovered [61].

In light of the dual role of environments in both inducing and suppressing entanglement, this paper examines the transition between ESD and ESB [Fig. 1(a)]. While this transition, often recognized as entanglement rebirth, has been explored in various contexts [58, 62–65], a common strategy to accomplish such a transition has been lacking. In this study, we introduce the entanglement switch parameter (ESP) ε based on Bell states. The ESP is defined so that its sign indicates whether the entanglement is switched on or off. By assuming that a sufficiently small ESP does not affect the overall entanglement tendency but only slightly displaces the trajectories in the Hilbert space, we present a generic recipe for preparing initial states that yield the immediate onset of ESD or ESB. If the *additional* condition that the local time-even symmetry in the entanglement monotones is satisfied, a nontrivial (namely, finite) transition time can be achieved. This transition of finite duration (TFD) emerges in both pure and mixed states. Without loss of generality, we choose to investigate a simple model—perhaps the simplest—the spin-star Heisenberg model with two subsystems [Fig. 1(b)]. Each subsystem contains a spin-1/2 qubit, with the magnitude of the central spin effectively accounting for the environmental degrees of freedom. The simplicity of the model allows the arguments to be presented transparently, and even analytic results can be obtained. Nonetheless, other spin-product forms, such as the Dzyaloshinskii-Moriya interaction [58, 66], remain applicable. The findings herein provide guidelines for manipulating and controlling entanglement, offering a practical and systematic method that can be effectively adopted in designing and advancing quantum technology applications.

The paper is organized as follows. Section II describes the studied model and reviews the entanglement monotones. The results are discussed in Sec. III. We first examine the symmetries relevant to the occurrence of, and connections between, ESD, ESB, and the death-birth transition in Sec. III A. Section III B then outlines the recipe for achieving the transition utilizing initial Bell states with ESPs. The transition is inspected for both mixed states in Sec. III C and pure states in Sec. III D. Section IV summarizes the results.

II. MODEL AND ENTANGLEMENT MONOTONE

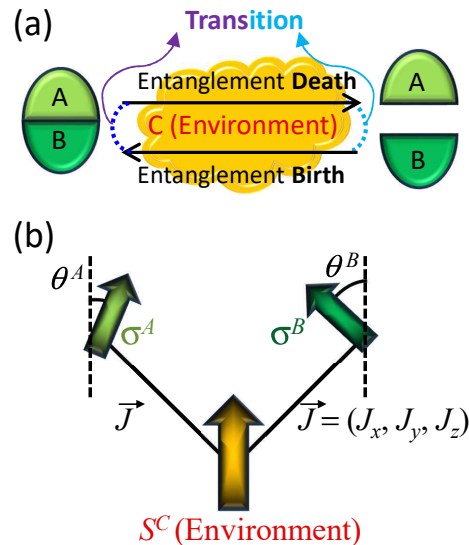


FIG. 1. (a) Schematic of the environment- C -induced bipartite A - B entanglement dynamics, including entanglement death (right arrow), entanglement birth (left arrow), transition from death to birth (blue dotted line), and transition from birth to death (purple dotted line). (b) Spin-star model illustrating two spin-1/2 subsystems, σ^A and σ^B , both coupled to a spin- S^C environment through Heisenberg exchange interactions \vec{J} (solid lines). The conventional spherical coordinate system is used with spin- z axis at $(\theta, \phi) = (0, 0)$; for example, the spin directions of A and B are represented by the polar angles θ_A and θ_B , respectively.

To realize ESD, ESB, and the transition between them in Fig. 1(a), consider the spin-star model in Fig. 1(b). This model consists of two spin-1/2 qubits, A and B , interacting with a common environment C through Heisenberg exchange coupling $\vec{J} = (J_x, J_y, J_z)$. The environment carrying quantum degrees of freedom with spin S^C , can be either pure $\text{Tr}[(\rho^C)^2] = 1$ or mixed $\text{Tr}[(\rho^C)^2] < 1$, where ρ^C represents the reduced density matrix (DM) for C . The Hamiltonian reads,

$$H_{\vec{J}} = \sum_{\alpha=x,y,z} J_{\alpha} S_{\alpha}^C \sigma_{\alpha}^A + J_{\alpha} S_{\alpha}^C \sigma_{\alpha}^B \quad (1)$$

in which σ_{α}^A and σ_{α}^B are Pauli matrices of the qubit subsystems, and S_{α}^C is the spin- S^C matrix in direction $\alpha \in \{x, y, z\}$, e.g., $S_{\alpha}^C = \sigma_{\alpha}^C/2$ if $S^C = 1/2$. The reduced Planck's constant \hbar is set to $\hbar = 1$ here. The time evolution operator $U(\vec{J}, t)$ governs the dynamics of the total wave function $|\psi(t)\rangle = U(\vec{J}, t)|\psi_0\rangle = |S^C, \sigma^A, \sigma^B\rangle(t)$, with

$$U(\vec{J}, t) = \exp(-iH_{\vec{J}}t), \quad (2)$$

rendering the equation of motion for the DM,

$$\frac{d}{dt}\varrho(t) = -i[H_{\vec{J}}, \varrho(t)], \quad (3)$$

where the commutator is defined as $[X, Y] \equiv XY - YX$. The initial state can be prepared with classical weights w_i via

$$\begin{aligned} \varrho(t=0) &= \varrho_0 \\ &= \sum_i w_i |\psi_i\rangle \langle \psi_i|, \end{aligned} \quad (4)$$

while with quantum weights $c_i = \sqrt{w_i}$ over the orthonormal basis $|\chi_i\rangle$ via

$$|\psi_0\rangle = \sum_i c_i |\chi_i\rangle. \quad (5)$$

From Eq. (3), the short-time (immediate) behavior of the system after interacting with the environment is then harnessed by the leading terms of the expansion,

$$\begin{aligned} \varrho(t) &= \varrho_0 + (-i)[H_{\vec{J}}, \varrho_0] dt \\ &\quad + \frac{1}{2!} (-i)^2 [H_{\vec{J}}, [H_{\vec{J}}, \varrho_0]] dt^2 \\ &\quad + O(dt^3). \end{aligned} \quad (6)$$

As depicted in Fig. 1(a), we are interested in the dynamics of bipartite entanglements between A and B , whose corresponding reduced DM reads,

$$\text{Tr}_C[\varrho(t)] = \rho^{AB}(t) \equiv \rho(t)$$

in which environment C is traced out. One of the entanglement monotones, which faithfully [67, 68] reflects the two-qubit entanglement, is the negativity [69]

$$\mathcal{N}(\vec{J}, t) = \text{Tr} \sqrt{\rho^{TB}(t)^\dagger \rho^{TB}(t)}, \quad (7)$$

computed as the absolute sum of all negative eigenvalues of the partial transpose

$$[\rho^{TB}(t)]_{ab, a'b'} = \rho_{ab', a'b}(t). \quad (8)$$

Here subscripts a and a' (b and b') denote the indices belonging to A (B). The negativity $\text{Tr} \sqrt{\rho^{TA}(t)^\dagger \rho^{TA}(t)} = \text{Tr} \sqrt{\rho^{TB}(t)^\dagger \rho^{TB}(t)}$ is irrelevant to which subsystem is transposed. In the case of two qubits, another equivalent entanglement monotone, called the concurrence [70–72] \mathcal{C} can also be used to quantify entanglement by finding the maximum,

$$\mathcal{C}(\vec{J}, t) = \max\{0, 2\gamma_{\max} - \Gamma\} \quad (9)$$

with $\gamma \in \{\gamma_1, \gamma_2, \gamma_3, \gamma_4\}$ being the eigenvalues of the matrix $\sqrt{\sqrt{\rho(t)}\rho'(t)\sqrt{\rho(t)}}$, $\gamma_{\max} = \max(\gamma)$, and $\Gamma = (\gamma_1 + \gamma_2 + \gamma_3 + \gamma_4)$. Here $\rho'(t)$ is constructed, from the

complex conjugate $\rho^*(t)$ of the four-by-four reduced DM $\rho(t)$ and the tensor product $\sigma_y^{\otimes 2} = \sigma_y \otimes \sigma_y$, as

$$\rho'(t) = \sigma_y^{\otimes 2} \rho(t)^* \sigma_y^{\otimes 2}.$$

Being worth mentioning, the evolved density matrix, $\varrho(t)$ and reduced DM, $\rho(t)$, $\rho^{TA}(t)$, and $\rho^{TB}(t)$, depend on the interaction \vec{J} , whereas the initial DM ϱ_0 and the reduced bipartite ρ_0 do not. As we will see later, the immediacy to encounter ESD and ESB can be controlled primarily by the interaction-independent ESP ε solely encoded in the initial conditions.

III. RESULT AND DISCUSSION

We begin with analyzing how entanglement responds to different symmetries. Even in the special case of direct A - B exchange,

$$H_{\vec{J}}^{dir} = \sum_{\alpha=x,y,z} J_{\alpha}^{dir} \sigma_{\alpha}^A \sigma_{\alpha}^B$$

we gain valuable insights into how the anisotropy of exchange \vec{J} induces entanglement. Using an expansion similar to Eq. (6), the immediate (near-future $dt \approx 0$) concurrence can be computed straightforwardly as,

$$\mathcal{C}^{dir}(\vec{J}^{dir}, dt) = 2|dt(J_y^{dir} - J_x^{dir} \cos \theta_B)| + O(dt^2), \quad (10)$$

with defining σ^A in spin- z , $\theta_A \equiv 0$, and θ_B being the angle between the two initial unentangled spin directions. It is interesting to note that the immediate entanglement does not depend on the out-of-plane J_z^{dir} but solely on the in-plane J_x^{dir} and J_y^{dir} . If two initial spins are both in spin- z , $\theta_B = 0$, then isotropic $J_x^{dir} = J_y^{dir}$ does not elicit any entanglement. However, if in-plane exchange is anisotropic (i.e., spin configuration of lowest energy prefers some special in-plane directions), entanglement $\mathcal{C}^{dir}(\vec{J}^{dir}, dt) > 0$ emerges. If σ^A and σ^B are not collinear, $\vec{n}^A \times \vec{n}^B \neq 0$, then entanglement can be easily evoked as indicated by the coordinate-free form of Eq. (10),

$$\begin{aligned} &\mathcal{C}^{dir}(\vec{J}^{dir}, dt) \\ &\approx 2|dt| \times \left| \vec{J}^{dir} \cdot (\vec{n}^A \times \vec{n}^B) \right. \\ &\quad \left. + \vec{J}^{dir} \cdot [\vec{n}^A \times (\vec{n}^A \times \vec{n}^B)] (\vec{n}^A \cdot \vec{n}^B) \right|, \end{aligned} \quad (11)$$

where $\vec{n}^{A/B}$ is the unit vector in the initial spin $\sigma^{A/B}$ direction. Furthermore, within the small interval $[-dt, dt]$, the prefactor $|dt|$ in the monotone (11) implies the local (around $t \approx 0$) time-even symmetry, $\mathcal{C}^{dir}(\vec{J}^{dir}, dt) = \mathcal{C}^{dir}(\vec{J}^{dir}, -dt)$. While in the above case the entanglement death-birth transition is trivial, i.e., of zero duration, as we will see later, this symmetry is instrumental in constructing the immediate TFD using the ESP.

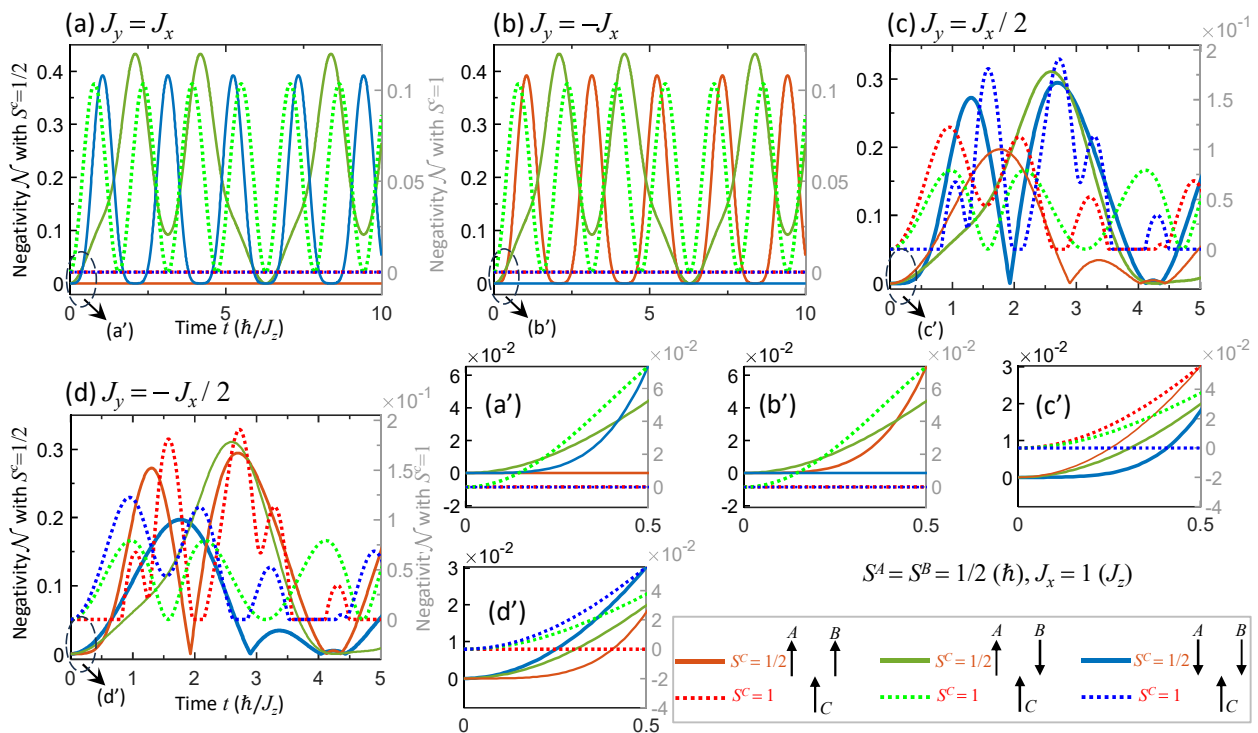


FIG. 2. Evolution of entanglement negativity, $\mathcal{N}(\vec{J}, t)$, for the initial unentangled spin states $|S^C, \sigma^A, \sigma^B\rangle = |\uparrow, \uparrow, \uparrow\rangle$ (red), $|\uparrow, \uparrow, \downarrow\rangle$ (green), and $|\uparrow, \downarrow, \downarrow\rangle$ (blue) with $S^C = 1/2$ (solid lines, left axis) and $S^C = 1$ (dotted lines, right axis), at different exchange coupling, (a) $\vec{J} = (1, 1, 1)$, (b) $\vec{J} = (1, -1, 1)$, (c) $\vec{J} = (1, 0.5, 1)$, and (d) $\vec{J} = (1, -0.5, 1)$, in units of $J_z \equiv 1$. Corresponding zoomed-in views around $t = 0$, consistent with the expressions in Table I, are shown in (a'), (b'), (c'), and (d'). Note that the blue (red) solid line in (a) [(b)] shows that the negativity initially grows at an order higher than dt^2 before oscillating periodically, i.e., no finite-duration transitions are found for all cases of $S^C = 1/2$ within the chosen time window.

TABLE I. Early development of the characteristic negative eigenvalue $\lambda^*(dt)$ for different all unentangled and pure initial spin configurations $|S^C, \sigma^A, \sigma^B\rangle$, as a function of the environment spin S^C . The highest spin-z eigenstate of C is represented by $|\uparrow, \sigma^A, \sigma^B\rangle = |m = S^C, \sigma^A, \sigma^B\rangle$.

Configuration $ S^C, \sigma^A, \sigma^B\rangle$	Characteristic negative eigenvalue $\lambda^*(dt)$
$ \uparrow, \uparrow, \uparrow\rangle$	$dt^2 S^C \times \begin{cases} J_y (J_y - J_x), & \text{if } J_x > J_y \\ J_x (J_x - J_y), & \text{if } J_x < J_y \end{cases} + O(dt^3), \text{ sign}(J_x) = \text{sign}(J_y)$
$ \uparrow, \uparrow, \downarrow\rangle$	$dt^2 S^C \left(J_x^2 + J_y^2 - \sqrt{(J_x^2 + J_y^2)^2 + 4J_x^2 J_y^2} \right) + O(dt^3)$
$ \uparrow, \downarrow, \downarrow\rangle$	$dt^2 S^C \times \begin{cases} J_y (J_x + J_y), & \text{if } J_x > J_y \\ J_x (J_x + J_y), & \text{if } J_x < J_y \end{cases} + O(dt^3), \text{ sign}(J_x) = -\text{sign}(J_y)$

Now, let us return to the environment-mediated case (1) and focus on the negativity (7). Unless otherwise specified, throughout this paper, for all initial states studied in the limit $dt \rightarrow 0^+$, there is at most a single negative eigenvalue of ρ^{TB} , Eq. (8), which we define as the *characteristic negative eigenvalue* (CNE) $\lambda^*(dt)$.

This eigenvalue determines whether the system exhibits immediate negativity,

$$\mathcal{N}(\vec{J}, dt) = \max\{0, -\lambda^*(dt)\}.$$

For different S^C and for *all unentangled and pure* initial states $|S^C, \sigma^A, \sigma^B\rangle = |\uparrow, \uparrow, \uparrow\rangle$, $|\uparrow, \uparrow, \downarrow\rangle$, and $|\uparrow, \downarrow, \downarrow\rangle$, using expansion (6), we compute the CNE in Table I. The $|\uparrow, \sigma^A, \sigma^B\rangle = |m = S^C, \sigma^A, \sigma^B\rangle$ denotes C in its highest spin-z eigenstate. The corresponding negativity dynamics is shown in Fig. 2, where exchange $J_z = 1$ is adopted. Although the currently discovered physical exchange interactions are limited (see, for example, Table I in Ref. [73]), Fig. 2 suggests that ESD and ESB can be induced for various types of \vec{J} . However, for all $S^C = 1/2$, represented by the solid lines, the transition durations are trivial within the chosen time window; that is, no TFD is observed. The zero durations are also verified by examining the concurrence $\mathcal{C}(\vec{J}, t)$ (not shown here). Specifically, the $|\uparrow, \uparrow, \uparrow\rangle$ blue solid line in Fig. 2(a) [the $|\uparrow, \downarrow, \downarrow\rangle$ red solid lines in Fig. 2(b)] indicates that the negativity initially develops at an order higher than dt^2 , as inferred from Table I, and then undergoes periodic oscillation. In addition, Fig. 2 shows that when an opposite

sign is assigned in the in-plane exchange, $J_y \rightarrow -J_y$, the environmental spin field is effectively reversed, turning the negativity of the initial state from $|\uparrow, \uparrow, \uparrow\rangle$ (blue lines) into that of $|\uparrow, \downarrow, \downarrow\rangle$ (red lines). Although no immediate TFD is seen in Fig. 2, the TFD can still be found after a sufficient wait; for instance, see the blue and red dotted lines ($S^C = 1$) around $t = 4$ in Figs. 2(c) and 2(d). One can thus monitor the entanglement until the TFD emerges and identify the states at the onset of the transition. However, these states, along with the transition beginning time and the transition duration identified through this monitoring process, are case-dependent and difficult to control. As will be seen later, a systematic method for identifying the states leading to TFD can be established. Before addressing this method, it is worth discussing how symmetry can be applied to relate ESD and ESB in systems with the same or different \vec{J} .

A. Symmetry analysis

It is evident from Eq. (2) that the parameter t can be absorbed into \vec{J} in the spin-star model (1) as $U(\vec{J}, t) = U(\vec{J}t, 1)$, leading to

$$U(\vec{J}, -t) = U(-\vec{J}, t). \quad (12)$$

Hence, the effect of the swap $\vec{J} \rightarrow -\vec{J}$ is equivalent to running the time backward. As a consequence, the existence of ESD (ESB) in the \vec{J} environmental exchange reflects the presence of ESB (ESD) in $-\vec{J}$. The death-to-birth (birth-to-death) transition in \vec{J} guarantees the birth-to-death (death-to-birth) transition in $-\vec{J}$. In other words, a process in $\vec{J} < 0$ ferromagnets ensures the occurrence of the reverse process in the corresponding $\vec{J} > 0$ antiferromagnets.

Another similar dynamic reversal can be argued based on the time-reversal symmetry, which our current system possesses. Let \mathcal{T} be the time-reversal operator, and consider a system that obeys the time-reversal symmetry $\mathcal{T}H(t)\mathcal{T}^\dagger = H(t)$, with $H(t) = H_{\vec{J}}$ in our case. Applying \mathcal{T} to the equation of motion (3) yields,

$$\frac{d}{dt}\bar{\varrho}(\bar{t}) = i[H(\bar{t}), \bar{\varrho}(\bar{t})], \quad (13)$$

with $\bar{t} \equiv -t$. This means that the same equation of motion in a *rewound* form of (3) governs $\bar{\varrho}(\bar{t})$. Accordingly, at any given time t , by preparing the initial state $\bar{\varrho}(\bar{t}) = \mathcal{T}\varrho(t)\mathcal{T}^\dagger$ —which corresponds to flipping all the spins in the eigenspinors that decompose $\varrho(t)$ —one can recover the original initial negativity $\mathcal{N}(t = 0)$. That is, if the initial state ϱ_0 evolves at time t after encountering ESD (ESB), then the final-as-initial reversal state $\mathcal{T}\varrho(t)\mathcal{T}^\dagger$ will visit ESB (ESD) in the same system.

Furthermore, the symmetry that resides in the vicinity of the entanglement-unentanglement boundary is the local time-even symmetry,

$$\mathcal{N}(\vec{J}, dt) = \mathcal{N}(\vec{J}, -dt), \quad (14)$$

or simply dt^2 symmetry as referred to herein. This symmetry is characterized by the dt -dependent leading order dt^{2n} , with $n = 1, 2, \dots$, of the monotone. Unlike time-reversal symmetry, the dt^2 symmetry depends on the initial state. We elaborate further on the dependence of negativity on dt below. Note that a partial trace over C must be performed to obtain the reduced DM ρ . Since ρ is a four-by-four matrix, expanding to the second term in (6) contributes to $\mathcal{N}(\vec{J}, dt)$ up to the fourth order, dt^4 , while the third term contributes at orders dt^2 , dt^4 , dt^6 , and dt^8 . Therefore, it is sufficient to show that $\mathcal{N}(\vec{J}, dt)$ is at least of order dt^2 if the expansion up to the second term in Eq. (6) does not yield any linear dt term in $\mathcal{N}(\vec{J}, dt)$.

The dt^2 symmetry corresponds to the trajectories p_1 or p_2 approaching the entanglement-unentanglement boundary in the Hilbert space, as shown schematically in Fig. 3. The trajectories p_1 and p_2 in Fig. 3 imply trivial transition. The nontrivial transition with ESD or ESB around $t = 0$, requires the monotone to have a leading dt -dependence term of order dt^{2n-1} . For example, p_0 in Fig. 3 indicates the occurrence of ESD. However, dt^2 symmetry actually appears in a wide variety of initial states. Table I already shows that dt^2 symmetry manifests in all unentangled and pure initial states. In fact, unentangled mixed initial states of the form,

$$\varrho_0 = \rho^C \otimes |\sigma^A\rangle\langle\sigma^A| \otimes |\sigma^B\rangle\langle\sigma^B|, \quad (15)$$

also exhibit dt^2 symmetry. Here ρ^C is in diagonal form,

$$\rho^C = \begin{pmatrix} \rho_{S^C}^C & & & 0 \\ & \rho_{S^C-1}^C & & \\ & & \ddots & \\ 0 & & & \rho_{-S^C+1}^C \\ & & & & \rho_{-S^C}^C \end{pmatrix}.$$

Denoting the initial spin directions of $\sigma^{A/B}$ by $(\theta^{A/B}, \phi^{A/B})$ in spherical coordinates, and taking terms up to the second in (6), the CNE for initial states (15) can be computed as,

$$\begin{aligned} \lambda^* &= dt^2 \frac{J_z^2}{2} \\ &\times \left(\sum_{m=-S^C, -S^C+1, \dots, S^C-1, S^C} m \rho_m^C \right)^2 \\ &\times (-2 + \cos 2\theta_A + \cos 2\theta_B) + O(dt^2). \end{aligned} \quad (16)$$

Note that the remaining $O(dt^2)$ above originates from the third term in expansion (6).

The dt^2 symmetry also shows up in the A - B entangled pure initial states of the form, $|\psi_0\rangle = |\uparrow\rangle \otimes |\alpha_p^\pm\rangle$, $|\uparrow\rangle \otimes |\alpha_p^+\rangle$, $|\uparrow\rangle \otimes |\beta_p^\pm\rangle$, and $|\uparrow\rangle \otimes |\beta_p^-\rangle$. Here,

$$|\alpha_p^\pm\rangle = \sqrt{\frac{1+p}{2}} |\uparrow, \uparrow\rangle \pm \sqrt{\frac{1-p}{2}} |\uparrow, \downarrow\rangle$$

and

$$|\beta_p^\pm\rangle = \sqrt{\frac{1+p}{2}} |\uparrow, \downarrow\rangle \pm \sqrt{\frac{1-p}{2}} |\uparrow, \uparrow\rangle$$

are the partially ($0 < p < 1$) or fully ($p = 0$) entangled Bell states. Again, considering *up to the second term* in (6), the CNE for different S^C varies with dt^2 as,

$$\lambda^* = \frac{-\sqrt{1-p^2}}{2} \left[1 + 8 (S^C J_z dt)^2 \right] + O(dt^2) \quad (17)$$

for $|\alpha_p^\pm\rangle$ and

$$\lambda^* = \frac{-\sqrt{1-p^2}}{2} + O(dt^2) \quad (18)$$

for $|\beta_p^\pm\rangle$. Therefore, the entanglement remains for small dt , namely, no immediate ESD. At first glance, it appears that dt^2 symmetry exists in abundant initial conditions as shown above but does not lead to any ESD, ESB, and TFD. However, if a parameter ε is introduced to slightly shift the symmetry point of the dt^2 symmetry, then immediate transitions can actually be fulfilled. We will show below that this shift is feasible. One can deviate the initial states away from the entanglement-entanglement boundary through appropriate constructions using fully entangled Bell states.

$$|\alpha_p^\pm\rangle \equiv |\alpha_{p=0}^\pm\rangle$$

and

$$|\beta_p^\pm\rangle \equiv |\beta_{p=0}^\pm\rangle.$$

B. Recipe for immediate entanglement death-birth transition in Bell states

We discuss the recipe for preparing initial states at desired quantum configurations near the entanglement-entanglement boundary for the realization of ESD and ESB illustrated in Fig. 3. Consider the initial reduced DM,

$$\begin{aligned} \rho_0 = & w_{\alpha^+} |\alpha^+\rangle \langle \alpha^+| \\ & + w_{\alpha^-} |\alpha^-\rangle \langle \alpha^-| \\ & + w_{\beta^+} |\beta^+\rangle \langle \beta^+| \\ & + w_{\beta^-} |\beta^-\rangle \langle \beta^-|, \end{aligned} \quad (19)$$

with the weighting $W = (w_{\alpha^+}, w_{\alpha^-}, w_{\beta^+}, w_{\beta^-})$ being normalized, $w_{\alpha^+} + w_{\alpha^-} + w_{\beta^+} + w_{\beta^-} = 1$. Through

straightforward computations, we find that the eigenvalues of the partial transpose, ρ_0^{TB} in (8), are $\lambda = 1/2 - w_{\alpha^+}$, $1/2 - w_{\alpha^-}$, $1/2 - w_{\beta^+}$, and $1/2 - w_{\beta^-}$. The negativity \mathcal{N} thus aligns with the concurrence \mathcal{C} in Eq. (9), with the γ evaluated as $\gamma \in \{w_{\alpha^+}, w_{\alpha^-}, w_{\beta^+}, w_{\beta^-}\}$; both monotones signify the presence of entanglement if any of the weights $w_{\alpha^{+/-}}$ and $w_{\beta^{+/-}}$ exceed one-half. Also, the CNE is well-defined because ρ_0^{TB} has at most one negative eigenvalue. If only two weights are employed in Eq. (19), there is always one negative eigenvalue in λ when none of the weights equals one-half. In this case, we can introduce the ESP ε to assign the weighting as $\{1/2 + \varepsilon/2, 1/2 - \varepsilon/2\}$. Accordingly, $\text{sign}(\varepsilon) \neq 0$ switches on the entanglement, corresponding to p_3 and p_6 in Fig. 3(b), while $\text{sign}(\varepsilon = 0) \equiv 0$ switches off the entanglement, corresponding to p_1 and p_2 in Fig. 3(a). If more than two Bell states are adopted, entanglement can be switched by incorporating $1/2 + \varepsilon/2$ in one of the weights. For example, assign the weighting $\{1/2 + \varepsilon/2, 1/4 - \varepsilon/4, 1/4 - \varepsilon/4\}$ in Eq. (19) for involving three Bell states and $\{1/2 + \varepsilon/2, 1/6 - \varepsilon/6, 1/6 - \varepsilon/6, 1/6 - \varepsilon/6\}$ for involving four. We say that the ESP ε is penetrable if opposite signs of ε generate correspondingly entangled and unentangled *initial* states, i.e., $\varepsilon \rightarrow -\varepsilon$ permits penetration of the state through the boundary. In the above preparation involving more than two Bell states, it is evident that the penetrability of the ESP can be accomplished. As a result, assuming the trajectory's tendency (toward entanglement or unentanglement) remains unchanged under a small enough ε , the swap $\varepsilon \rightarrow -\varepsilon$ (the sign of ε) can always be designed to yield $p_3 \rightarrow p_4$ and $p_5 \rightarrow p_6$, reaching the desired p_4 for ESB and p_6 for ESD. Moreover, if the dt^2 symmetry is also satisfied, the whole (including $t < 0$) trajectories, $p_{1,2,\dots,6}$ in Fig. 3, is valid; one thus attains a death-to-birth transition p_4 and a birth-to-death transition p_6 .

Accordingly, the recipe for observing the TFD proceeds as follows: (i) Prepare initial states with the weighting W , as described above, using a trial sign for ε . (ii) If ESD and ESB are not observed in the near future, swap the sign $\varepsilon \rightarrow -\varepsilon$. (iii) Check if the system has any of the symmetries depicted in (12), (13), and (14); utilize (12) or (13) to convert ESD into ESB or vice versa and utilize (14) to attain the death-birth transition. Being worth mentioning, the recipe for realizing the ESD and ESB described above does not rely on specific types of interacting Hamiltonians. Although when adopting only two weighted Bell states the ESP is not penetrable (i.e., entanglement persists for both positive and negative ε , and hence the recipe may fail), there is still a chance to witness the nontrivial transition p_6 , as demonstrated below.

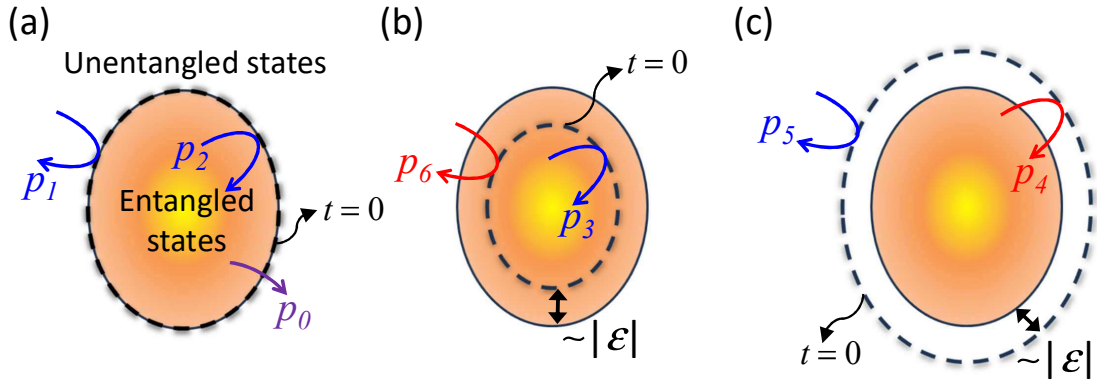


FIG. 3. Schematic in the Hilbert space for the trajectories, p_0, p_1, \dots , and p_6 , approaching the boundary between entangled (colored inner region) and unentangled (colorless outer region) states near the initial time $t = 0$ (dashed lines). (a) $t = 0$ is set at the boundary, (b) $t = 0$ is set slightly toward the entangled region, quantified by $|\epsilon|$, and (c) $t = 0$ is set slightly toward the unentangled region, also quantified by $|\epsilon|$. The entanglement switch parameter ϵ is penetrable if it has opposite signs in (b) and (c), such that $\epsilon \rightarrow -\epsilon$ shifts p_3 and p_5 to p_6 and p_4 , respectively. For trajectories $p_{1,2,\dots,6}$, the local time-even symmetry in entanglement monotonies allows the validity of the entire trajectory. However, if the system lacks this symmetry, half of the trajectory of $t > 0$ remains applicable.

TABLE II. Immediate evolution of characteristic negative eigenvalue $\lambda^*(dt)$ for different mixing weightings, $W_{1,2,\dots,6}$ incorporating two Bell states, $W_{7,8,\dots,10}$ three Bell states, and $W_{11,12,\dots,14}$ four Bell states in Eq. (19). The environment has $S^C = 1/2$ initially at spin- z up. The chosen sign of ϵ is listed in the second column, with the corresponding trajectory (see Fig. 3) approaching the entanglement-unentanglement boundary shown in the last column. Here for W_6 , specifically, the leading term in $-O(dt^4/\epsilon)$ is $-dt^4 J_x^2 J_y^2 (1 + \epsilon) (3 + 7\epsilon) / (12\epsilon)$ and $O(dt^4/\epsilon)$ is $dt^4 J_x^2 J_y^2 (1 + \epsilon)^2 / (4\epsilon)$.

Weighting ($w_{\alpha^+}, w_{\alpha^-}, w_{\beta^+}, w_{\beta^-}$)	Sign of entanglement switch parameter ϵ	Characteristic negative eigenvalue $\lambda^*(dt)$	Approaching trajectory
$W_1 = (\frac{1+\epsilon}{2}, \frac{1-\epsilon}{2}, 0, 0)$	+	$\frac{-\epsilon}{2} + dt^2 \frac{J_x^2(1+\epsilon)}{2}$	p_6
$W_2 = (\frac{1+\epsilon}{2}, 0, \frac{1-\epsilon}{2}, 0)$	+	$\frac{-\epsilon}{2} + dt^2 J_x^2 \epsilon$	p_6
$W_3 = (\frac{1+\epsilon}{2}, 0, 0, \frac{1-\epsilon}{2})$	+	$\frac{-\epsilon}{2} + dt^2 \frac{J_y^2(1+\epsilon)}{2}$	p_6
$W_4 = (0, \frac{1+\epsilon}{2}, \frac{1-\epsilon}{2}, 0)$	+	$\frac{-\epsilon}{2} + dt^2 J_y^2 \epsilon$	p_6
$W_5 = (0, \frac{1+\epsilon}{2}, 0, \frac{1-\epsilon}{2})$	+	$\frac{-\epsilon}{2} + dt^2 \frac{J_y^2(1+\epsilon)}{2}$	p_6
$W_6 = (0, 0, \frac{1+\epsilon}{2}, \frac{1-\epsilon}{2})$	\pm	$\frac{-\epsilon}{2} + dt^2 \frac{(1+\epsilon)(J_x^2 + J_y^2)}{2} - O\left(\frac{dt^4}{\epsilon}\right)$, if $\epsilon > 0$ $\frac{\epsilon}{2} + O\left(\frac{dt^4}{\epsilon}\right)$, if $\epsilon < 0$	p_3
$W_7 = (\frac{1+\epsilon}{2}, \frac{1-\epsilon}{4}, \frac{1-\epsilon}{4}, 0)$	+	$\frac{-\epsilon}{2} + dt^2 \frac{J_x^2(1+3\epsilon)}{4}$	p_6
$W_8 = (0, \frac{1+\epsilon}{2}, \frac{1-\epsilon}{4}, \frac{1-\epsilon}{4})$	+	$\frac{-\epsilon}{2} + dt^2 \frac{J_y^2(1+3\epsilon)}{4}$	p_6
$W_9 = (\frac{1-\epsilon}{4}, 0, \frac{1+\epsilon}{2}, \frac{1-\epsilon}{4})$	+	$\frac{-\epsilon}{2} + dt^2 \left[\frac{J_x^2(1+3\epsilon)}{4} + \frac{J_y^2(1+\epsilon)}{2} \right]$	p_6
$W_{10} = (\frac{1-\epsilon}{4}, \frac{1-\epsilon}{4}, 0, \frac{1+\epsilon}{2})$	-	$\frac{-\epsilon}{2} - dt^4 \frac{J_x^2 J_y^2 (-1+\epsilon)^2}{8(1+\epsilon)}$	p_4
$W_{11} = (\frac{1+\epsilon}{2}, \frac{1-\epsilon}{6}, \frac{1-\epsilon}{6}, \frac{1-\epsilon}{6})$	+	$\frac{-\epsilon}{2} + dt^2 \frac{J_x^2(1+2\epsilon)}{3}$	p_6
$W_{12} = (\frac{1-\epsilon}{6}, \frac{1+\epsilon}{2}, \frac{1-\epsilon}{6}, \frac{1-\epsilon}{6})$	+	$\frac{-\epsilon}{2} + dt^2 \frac{J_y^2(1+2\epsilon)}{3}$	p_6
$W_{13} = (\frac{1-\epsilon}{6}, \frac{1-\epsilon}{6}, \frac{1+\epsilon}{2}, \frac{1-\epsilon}{6})$	+	$\frac{-\epsilon(1+2\epsilon)}{2+4\epsilon} + dt^2 \frac{J_x^2(1+4\epsilon+4\epsilon^2) + J_y^2(1+2\epsilon)^2}{3+6\epsilon}$	p_6
$W_{14} = (\frac{1-\epsilon}{6}, \frac{1-\epsilon}{6}, \frac{1-\epsilon}{6}, \frac{1+\epsilon}{2})$	-	$\frac{-\epsilon}{2} - dt^4 \frac{J_x^2 J_y^2 (-1+\epsilon)^2}{3+6\epsilon}$	p_4

C. Immediate transition with classical weighting (mixed states)

To demonstrate the recipe for mixed states $Tr(\rho_0^2) < 1$, we present analytic results based on (6) and numerical simulations on (3). We choose $S^C = 1/2$ at spin up $|\uparrow\rangle$

and the initial DM

$$\rho_0 = |\uparrow\rangle\langle\uparrow| \otimes \sum_{i=\alpha^+, \alpha^-, \beta^+, \beta^-} w_i |i\rangle\langle i|$$

of the classical mixing weights (4) specifically listed in Table II, where analytic expressions of entanglement dynamics are provided. Table II expands $\lambda^*(dt)$ up to

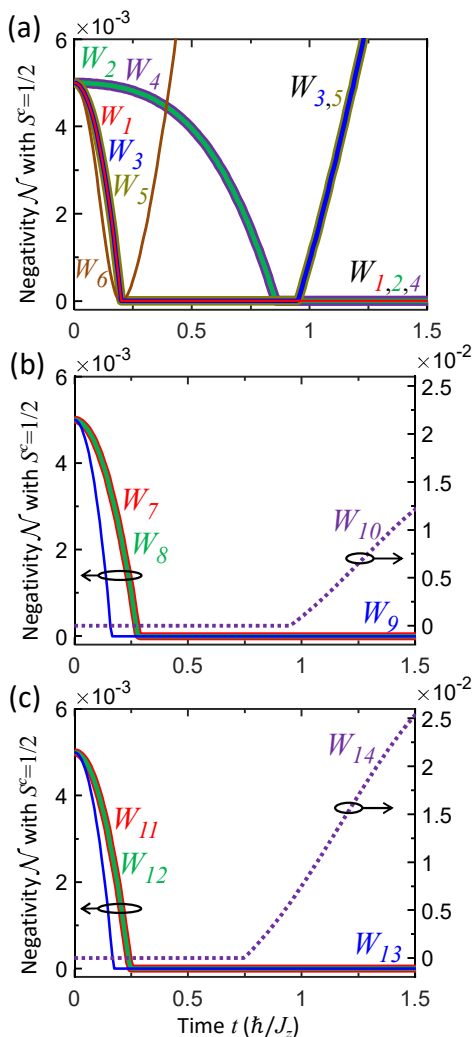


FIG. 4. Negativity development in mixed states with $|\varepsilon| = 10^{-2}$ and ferromagnetic $\vec{J} = (-0.5, -0.5, -1)$. The environment carries quantum degrees of freedom $2S^C + 1 = 2$ initially aligned with spin- z up. The mixing weightings W s in Table II are adopted. In (a), (b), and (c), two, three, and four Bell states are used, respectively. Positive (solid lines, left axis) entanglement switch parameters $\varepsilon > 0$ are chosen for all W s, except for W_{10} and W_{14} (dotted lines, right axis). The near-past and near-future negativity obeys $\mathcal{N}(\vec{J}, dt) = \mathcal{N}(\vec{J}, -dt)$, although the $t \lesssim 0$ region is not shown.

the first two leading orders using two Bell states in the weightings W_1, W_2, \dots, W_5 , and W_6 , using three Bell states in W_7, W_8, W_9 , and W_{10} , while using four Bell states in W_{11}, W_{12}, W_{13} , and W_{14} . The desired sign of ε is selected to achieve immediate ESD or ESB, and consequently, a nontrivial TFD due to the dt^2 symmetry (see Table II). Furthermore, for our spin-star model, Table II indicates that nontrivial TFD can all be identified except for weighting W_6 , where ε is not penetrable. For weighting W_6 of small ε , the CNE $\lambda^*(dt)$ stays in trajectory p_3

for both signs of ε , where $\lambda^*(dt)$ is predominantly governed by $O(dt^4/\varepsilon)$ if $\varepsilon < 0$ and $-O(dt^4/\varepsilon)$ if $\varepsilon > 0$ (as given in Table II), while in trajectory p_2 if $\varepsilon = 0$. For W_{10} and W_{14} , the higher-order dt^4 term leads to ESB if $\varepsilon < 0$ is chosen, corresponding to trajectory p_6 of TFD. Interestingly, J_z is absent in determining the immediate dynamics of entanglement, similar to the case of direct exchange in Eq. (10).

The numerical simulation for the negativity is shown in Fig. 4, where we adopt $\vec{J} = (-0.5, -0.5, -1)$ and $|\varepsilon| = 10^{-2}$. The result coincides with Table II. In Fig. 4, the positive (solid lines, left axis) ESP ε for all W s is selected, except for W_{10} and W_{14} , where negative $\varepsilon < 0$ (dashed lines, right axis) offers ESB depicted by trajectory p_4 . Note that Fig. 4 does not plot the negativity in the near-past $t \lesssim 0$ region, which is actually identical to the negativity in the near-future $t \gtrsim 0$ region, attributed to the dt^2 symmetry provided in Table II. In other words, the immediate TFD is obtained with p_4 (death-to-birth) and p_6 (birth-to-death) by further including the near-past entanglement dynamics. For weighting W_6 in Fig. 4, the negativity $\mathcal{N}(\vec{J}, dt)$ first decreases due to dt^2 term and then increases due to the dt^4/ε term, in line with the expression in Table II. Moreover, as Table II implies, the immediate $\mathcal{N}(\vec{J}, dt)$ remains unaffected by the strength of J_z and the sign of \vec{J} in our spin-star model.

D. Immediate transition with quantum weighting (pure states)

Following the recipe outlined in Sec. III B, we demonstrate the existence of the immediate TFD for pure states $\text{Tr}(\varrho_0^2) = 1$, with $\varrho_0 = |\psi_0\rangle\langle\psi_0|$ in the form (5), provided ε is penetrable. Specifically, consider initial

$$|\psi_0\rangle = \sum_{\substack{i=\alpha^+, \alpha^-, \beta^+, \beta^- \\ w_i \neq 0}} \sqrt{w_i} |i^C\rangle \otimes |i\rangle. \quad (20)$$

where the summation accounts for only the nonzero weights $w_i \neq 0$ chosen from Table II. The $|i^C\rangle$ loops over the spin- z eigenspinors $|m\rangle$ of C in descending order, $|m = S^C\rangle, |S^C - 1\rangle, \dots$, and $|m = -S^C\rangle$; the $S^C = 1/2$ is set to match the number of nonzero w_i in each of the weightings $W_{1,2,\dots,6}$, $S^C = 1$ in $W_{7,8,\dots,10}$, and $S^C = 3/2$ in $W_{11,12,\dots,14}$. For example, according to Table II, for W_9 , we assign

$$\begin{aligned} |\psi_0\rangle = & \sqrt{\frac{1-\varepsilon}{4}} |m=1\rangle \otimes |\alpha^+\rangle \\ & + \sqrt{\frac{1+\varepsilon}{2}} |m=0\rangle \otimes |\beta^+\rangle \\ & + \sqrt{\frac{1-\varepsilon}{4}} |m=-1\rangle \otimes |\beta^-\rangle, \end{aligned}$$

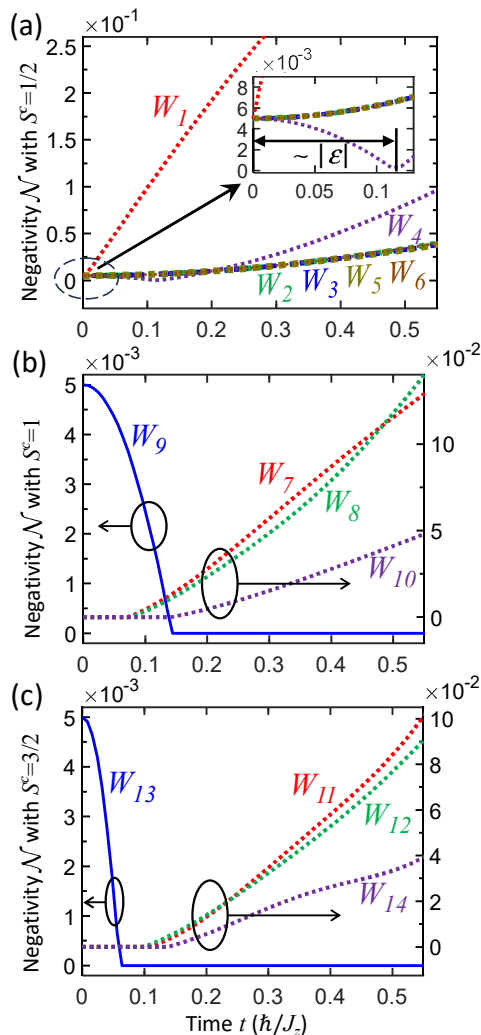


FIG. 5. Negativity development in pure states with $|\varepsilon| = 10^{-2}$ and ferromagnetic $\vec{J} = (-0.5, -0.5, -1)$. The environment possesses quantum degrees of freedom expanded by $2S^C + 1$ basis states with (a) $S^C = 1/2$, (b) $S^C = 1$, and (c) $S^C = 3/2$ associating with two, three, and four Bell states, respectively. The inset in (a) provides a zoomed-in view of W_4 around $t = 0$, with the local minimum of negativity occurring at the time $t \approx 0.11$ quantified by $|\varepsilon|$. The quantum weightings W s are assigned through Eq. (20) according to Table II. Solid (dotted) lines for the left (right) axis represent the adopted positive (negative) entanglement switch parameters $\varepsilon > 0$ ($\varepsilon < 0$). The near-past negativity $\mathcal{N}(\vec{J}, -dt)$ is identical to $\mathcal{N}(\vec{J}, dt)$.

while for W_{13} , we assign

$$\begin{aligned}
 |\psi_0\rangle = & \sqrt{\frac{1-\varepsilon}{6}} |m=3/2\rangle \otimes |\alpha^+\rangle \\
 & + \sqrt{\frac{1-\varepsilon}{6}} |m=1/2\rangle \otimes |\alpha^-\rangle \\
 & + \sqrt{\frac{1+\varepsilon}{2}} |m=-1/2\rangle \otimes |\beta^+\rangle \\
 & + \sqrt{\frac{1-\varepsilon}{6}} |m=-3/2\rangle \otimes |\beta^-\rangle.
 \end{aligned}$$

Because $|m\rangle \otimes |i\rangle$ constitutes an orthonormal basis, tracing out C in fact yields the same initial reduced DM, Eq. (19). Consequently, the previously established recipe remains applicable to the pure states (20) by associating different $|i^C\rangle$ with different $|m\rangle$, which avoids cross term like $|\alpha^\pm\rangle \langle\beta^\pm|$ in ρ_0 . Furthermore, employing again expansion (6) up to the second term, it can be shown that the pure states with the weights listed in Table II satisfy dt^2 symmetry.

Figure 5 plots the negativity for pure states with $\vec{J} = (-0.5, -0.5, -1)$ and $|\varepsilon| = 10^{-2}$. In the weightings W_1, W_2, \dots, W_5 , and W_6 , where only two Bell states are incorporated in ϱ_0 , the lack of penetrability of ε impedes the occurrence of ESD and ESB in Fig. 5(a). Neither sign of ε gives rise to a nontrivial transition such as p_6 . For example, W_4 in 5(a) with $\varepsilon < 0$ encounters a local minimum of negativity around $t \approx 0.11$. As ε is increased, at $\varepsilon = 0$ this local minimum is located exactly at $t = 0$ and becomes zero, indicating the absence of entanglement (trajectory p_2). With further increases to $\varepsilon > 0$, entanglement reappears at $t = 0$ (trajectory p_3). On the contrary, when more than two Bell states are utilized in ϱ_0 , the penetrability of ε expectedly enables the TFD, as demonstrated in Figs. 5(b) with three Bell states and 5(c) with four Bell states. The weightings W_9 and W_{13} , with positive $\varepsilon > 0$ (solid lines, left axis), render the entanglement birth-to-death transition (trajectory p_6), while other weightings with negative $\varepsilon < 0$ (dotted lines, right axis) result in the entanglement death-to-birth transition (trajectory p_4).

IV. SUMMARY

In summary, to identify the ESD, ESB, and TFD in Fig. 1, we propose a recipe for moving initial states around the entanglement-unentanglement boundary by introducing the ESP ε . The spin-star model of two qubits serves as an example to illustrate this recipe. To appreciate that the TFD is precious and nontrivial, we first examined the all unentangled and individually pure states in Table I and Fig. 2, where all *immediate* transitions, characterized by the nonzero CNE $\lambda^*(dt)$, exhibit *zero* duration (trajectory p_2 in Fig. 3). When ρ^C is a mixed state in a similar all unentangled configuration, the $\lambda^*(dt)$ in Eq. (16), depicts again trivial transition

(trajectory p_2). When C state and A - B state are both pure, where A - B is described by one Bell state unentangled with C , the leading term of finite constant in Eqs. (17) and (18) even implies no immediate transitions.

Viewing the local time-even (dt^2) symmetry Eq. (14) of p_2 as difficult to avoid, and examining all other trajectories in Fig. 3, we then realized that we can leverage this symmetry instead of avoiding it to induce the ESD and ESB. Such a transition is achieved by shifting the symmetry point away from the boundary via ε , encoded in the weights of the Bell states Eq. (19). When more than two Bell states are adopted (see W_7 , W_2 , \dots , and W_{14} in Table II), the initial state is penetrable through the boundary controlled by $\text{sign}(\varepsilon)$. The penetrability enables the immediate occurrence of the ESD and ESB, and when the dt^2 symmetry is satisfied, it ensures the entanglement death-birth transition for both mixed ϱ_0 in Figs. 4(b) and 4(c) and pure ϱ_0 in Figs. 5(b) and 5(c). Other symmetries characterized by Eq. (12) and Eq. (13) allow conversion between ESD and ESB, and vice versa.

The recipe with the swap $\varepsilon \rightarrow -\varepsilon$ works generally in any interactions, under the conditions that (i) ε is penetrable, and (ii) sufficiently small ε will only displace the trajectories without altering the entanglement tendency. Here both conditions hold when more than two Bell states are employed. However, the latter condition is valid only in certain cases using two Bell states; for example, see $\lambda^*(dt)$ with weightings, W_1 , W_3 , and W_5 in Table II corresponding to p_6 [as also seen in Fig. 4(a)].

The penetrability is lost when only two Bell states are used to construct ϱ_0 .

In the case of pure ϱ , $S^C = 1/2$ [solid lines in Fig. 2 and dashed lines in Fig. 5(a)], all transitions remain trivial, and no ESD and ESB are obtained with our recipe. We thus conjecture that, to observe the TFD, ESD, or ESB for a pure ϱ , the environment must possess quantum degrees of freedom greater than those of a qubit, namely, $2S^C + 1 > 2$. Nonetheless, extending this conjecture beyond the two Bell states used here would require a rigorous proof, which is beyond the scope of this paper. Furthermore, a phase prefactor $\exp(i\varphi_i)$ can be introduced in the construction Eq. (20), which leaves ρ_0 unchanged; thus, the prefactor is not relevant to the overall recipe. The phase φ_i was neglected in this paper, as discussing the effects from it would divert the focus herein. Even so, we believe the unveiled recipe will attract attention in the study of identifying and observing ESB and ESD. In particular, benefiting from the controllable duration of entanglement as well as its immediacy of occurrence, this recipe will assist in the engineering and application of entanglement dynamics. Furthermore, the introduced ESP, particularly the concept of penetrability, will open up new avenues for exploring the fundamental physics of entanglement kinetics.

ACKNOWLEDGMENTS

The author thanks Shih-Jye Sun, Ming-Chien Hsu, and Ching-Ray Chang for valuable discussions. S.-G. Tan is supported by the National Science and Technology Council of Taiwan under Grant. No: 113-2112-M-034-002.

-
- [1] R. Horodecki, P. Horodecki, M. Horodecki, and K. Horodecki, Rev. Mod. Phys. **81**, 865 (2009), URL <https://link.aps.org/doi/10.1103/RevModPhys.81.865>.
 - [2] C. H. Bennett and D. P. DiVincenzo, nature **404**, 247 (2000).
 - [3] F. Y. Khalili and E. S. Polzik, Phys. Rev. Lett. **121**, 031101 (2018), URL <https://link.aps.org/doi/10.1103/PhysRevLett.121.031101>.
 - [4] E. Zeuthen, E. S. Polzik, and F. Y. Khalili, Physical Review D **100**, 062004 (2019).
 - [5] A. K. Ekert, Physical review letters **67**, 661 (1991).
 - [6] P. W. Shor and J. Preskill, Physical review letters **85**, 441 (2000).
 - [7] N. Gisin, G. Ribordy, W. Tittel, and H. Zbinden, Reviews of modern physics **74**, 145 (2002).
 - [8] C. H. Bennett, Physica Scripta **1998**, 210 (1998).
 - [9] D. P. DiVincenzo, Science **270**, 255 (1995).
 - [10] A. Steane, Reports on Progress in Physics **61**, 117 (1998).
 - [11] D. P. DiVincenzo, Fortschritte der Physik: Progress of Physics **48**, 771 (2000).
 - [12] T. D. Ladd, F. Jelezko, R. Laflamme, Y. Nakamura, C. Monroe, and J. L. O'Brien, nature **464**, 45 (2010).
 - [13] M. A. Nielsen and I. L. Chuang, *Quantum computation and quantum information* (Cambridge university press, 2010).
 - [14] L. S. Madsen, F. Laudenbach, M. F. Askarani, F. Rortais, T. Vincent, J. F. Bulmer, F. M. Miatto, L. Neuhaus, L. G. Helt, M. J. Collins, et al., Nature **606**, 75 (2022).
 - [15] S.-H. Chen, Phys. Rev. B **109**, 045308 (2024), URL <https://link.aps.org/doi/10.1103/PhysRevB.109.045308>.
 - [16] M. Schlosshauer, Physics Reports **831**, 1 (2019).
 - [17] E. Vicari, Phys. Rev. A **98**, 052127 (2018), URL <https://link.aps.org/doi/10.1103/PhysRevA.98.052127>.
 - [18] M. Arzano, V. D'Esposito, and G. Gubitosi, Communications Physics **6**, 242 (2023).
 - [19] K. O. Yashodamma and Sudha, Results in Physics **3**, 41 (2013).
 - [20] T. Yu and J. H. Eberly, Phys. Rev. Lett. **93**, 140404 (2004), URL <https://link.aps.org/doi/10.1103/PhysRevLett.93.140404>.
 - [21] T. Yu and J. Eberly, Optics Communications **264**, 393 (2006).
 - [22] T. Yu and J. Eberly, Physical review letters **97**, 140403 (2006).
 - [23] K. Ann and G. Jaeger, Phys. Rev. A **76**, 044101 (2007), URL <https://link.aps.org/doi/10.1103/PhysRevA.76.044101>.
 - [24] T. Yu and J. H. Eberly, Science **323**, 598 (2009).

- [25] M. P. Almeida, F. de Melo, M. Hor-Meyll, A. Salles, S. Walborn, P. S. Ribeiro, and L. Davidovich, *science* **316**, 579 (2007).
- [26] B. Bellomo, R. Lo Franco, and G. Compagno, *Phys. Rev. Lett.* **99**, 160502 (2007), URL <https://link.aps.org/doi/10.1103/PhysRevLett.99.160502>.
- [27] B. Bellomo, R. Lo Franco, and G. Compagno, *Phys. Rev. A* **77**, 032342 (2008), URL <https://link.aps.org/doi/10.1103/PhysRevA.77.032342>.
- [28] A. Al-Qasimi and D. F. V. James, *Phys. Rev. A* **77**, 012117 (2008), URL <https://link.aps.org/doi/10.1103/PhysRevA.77.012117>.
- [29] F. Wang, P.-Y. Hou, Y.-Y. Huang, W.-G. Zhang, X.-L. Ouyang, X. Wang, X.-Z. Huang, H.-L. Zhang, L. He, X.-Y. Chang, et al., *Phys. Rev. B* **98**, 064306 (2018), URL <https://link.aps.org/doi/10.1103/PhysRevB.98.064306>.
- [30] K. K. Sharma and V. P. Gerdt, *International Journal of Theoretical Physics* **59**, 403 (2020).
- [31] A. R. P. Rau, M. Ali, and G. Alber, *Europhysics Letters* **82**, 40002 (2008), URL <https://dx.doi.org/10.1209/0295-5075/82/40002>.
- [32] X.-F. Qian and J. H. Eberly, *Physics Letters A* **376**, 2931 (2012), ISSN 0375-9601, URL <https://www.sciencedirect.com/science/article/pii/S0375960112008936>.
- [33] S. Chakraborty and A. K. Sarma, *Phys. Rev. A* **100**, 063846 (2019), URL <https://link.aps.org/doi/10.1103/PhysRevA.100.063846>.
- [34] N. Awasthi, A. Singh, and D. Kumar Joshi, *Frontiers in Quantum Science and Technology* **2**, 1207793 (2023).
- [35] D. Braun, *Phys. Rev. Lett.* **89**, 277901 (2002), URL <https://link.aps.org/doi/10.1103/PhysRevLett.89.277901>.
- [36] M. S. Kim, J. Lee, D. Ahn, and P. L. Knight, *Phys. Rev. A* **65**, 040101 (2002), URL <https://link.aps.org/doi/10.1103/PhysRevA.65.040101>.
- [37] S. Schneider and G. J. Milburn, *Phys. Rev. A* **65**, 042107 (2002), URL <https://link.aps.org/doi/10.1103/PhysRevA.65.042107>.
- [38] F. Benatti, R. Floreanini, and M. Piani, *Phys. Rev. Lett.* **91**, 070402 (2003), URL <https://link.aps.org/doi/10.1103/PhysRevLett.91.070402>.
- [39] M. Hor-Meyll, A. Auyuanet, C. V. S. Borges, A. Aragão, J. A. O. Huguenin, A. Z. Khoury, and L. Davidovich, *Phys. Rev. A* **80**, 042327 (2009), URL <https://link.aps.org/doi/10.1103/PhysRevA.80.042327>.
- [40] A. A. Valido, D. Alonso, and S. Kohler, *Phys. Rev. A* **88**, 042303 (2013), URL <https://link.aps.org/doi/10.1103/PhysRevA.88.042303>.
- [41] M. H. M. Passos, W. F. Balthazar, A. Z. Khoury, M. Hor-Meyll, L. Davidovich, and J. A. O. Huguenin, *Phys. Rev. A* **97**, 022321 (2018), URL <https://link.aps.org/doi/10.1103/PhysRevA.97.022321>.
- [42] R. Hartmann and W. T. Strunz, *Quantum* **4**, 347 (2020).
- [43] Y. Chen, J. Hu, and H. Yu, *Physical Review D* **105**, 045013 (2022).
- [44] J. Kong, R. Jiménez-Martínez, C. Troullinou, V. G. Lucivero, G. Tóth, and M. W. Mitchell, *Nature communications* **11**, 2415 (2020).
- [45] O. Lunt and A. Pal, *Phys. Rev. Res.* **2**, 043072 (2020), URL <https://link.aps.org/doi/10.1103/PhysRevResearch.2.043072>.
- [46] X. Turkeshi, A. Biella, R. Fazio, M. Dalmonte, and M. Schiró, *Phys. Rev. B* **103**, 224210 (2021), URL <https://link.aps.org/doi/10.1103/PhysRevB.103.224210>.
- [47] T. Botzung, S. Diehl, and M. Müller, *Phys. Rev. B* **104**, 184422 (2021), URL <https://link.aps.org/doi/10.1103/PhysRevB.104.184422>.
- [48] H. Y. Yuan, Y. Cao, A. Kamra, R. A. Duine, and P. Yan, *Physics Reports* **965**, 1 (2022), ISSN 0370-1573, quantum magnonics: When magnon spintronics meets quantum information science, URL <https://www.sciencedirect.com/science/article/pii/S0370157322000977>.
- [49] G. Mathew, S. L. L. Silva, A. Jain, A. Mohan, D. T. Adroja, V. G. Sakai, C. V. Tomy, A. Banerjee, R. Goreti, A. V. N., et al., *Phys. Rev. Res.* **2**, 043329 (2020), URL <https://link.aps.org/doi/10.1103/PhysRevResearch.2.043329>.
- [50] P. Laurell, A. Scheie, C. J. Mukherjee, M. M. Koza, M. Enderle, Z. Tylczynski, S. Okamoto, R. Coldea, D. A. Tennant, and G. Alvarez, *Phys. Rev. Lett.* **127**, 037201 (2021), URL <https://link.aps.org/doi/10.1103/PhysRevLett.127.037201>.
- [51] A. Scheie, P. Laurell, A. M. Samarakoon, B. Lake, S. E. Nagler, G. E. Granroth, S. Okamoto, G. Alvarez, and D. A. Tennant, *Phys. Rev. B* **103**, 224434 (2021), URL <https://link.aps.org/doi/10.1103/PhysRevB.103.224434>.
- [52] A. Suresh, R. Soares, P. Mondal, J. Pires, J. Lopes, A. Ferreira, A. Feiguin, P. Plecháč, and B. Nikolić, *arXiv preprint arXiv:2210.06634* (2022).
- [53] J. Hales, U. Bajpai, T. Liu, D. R. Baykusheva, M. Li, M. Mitrano, and Y. Wang, *Nature Communications* **14**, 3512 (2023).
- [54] T. Liu, L. Xu, J. Liu, and Y. Wang, *arXiv preprint arXiv:2408.04876* (2024).
- [55] A. Suresh, R. D. Soares, P. Mondal, J. P. S. Pires, J. M. V. P. Lopes, A. Ferreira, A. E. Feiguin, P. Plecháč, and B. K. Nikolić, *Phys. Rev. A* **109**, 022414 (2024), URL <https://link.aps.org/doi/10.1103/PhysRevA.109.022414>.
- [56] F. Garcia-Gaitan and B. K. Nikolić, *Phys. Rev. B* **109**, L180408 (2024), URL <https://link.aps.org/doi/10.1103/PhysRevB.109.L180408>.
- [57] A. Hutton and S. Bose, *Phys. Rev. A* **69**, 042312 (2004), URL <https://link.aps.org/doi/10.1103/PhysRevA.69.042312>.
- [58] Z. Qiang, Z. Xiao-Ping, Z. Qi-Jun, and R. Zhong-Zhou, *Chinese Physics B* **18**, 3210 (2009).
- [59] W.-B. He and X.-W. Guan, *Chinese Physics Letters* **35**, 110302 (2018).
- [60] H. Mostafa, M. Abdel-Baset, H. Saeed, K. Youssef, P. M. Reza, and D. Mohammed, *Applied Physics B* **128**, 87 (2022).
- [61] X.-Z. Yuan, H.-S. Goan, and K.-D. Zhu, *Phys. Rev. B* **75**, 045331 (2007), URL <https://link.aps.org/doi/10.1103/PhysRevB.75.045331>.
- [62] Z. Ficek and R. Tanaś, *Phys. Rev. A* **74**, 024304 (2006), URL <https://link.aps.org/doi/10.1103/PhysRevA.74.024304>.
- [63] Z. Ficek and R. Tanaś, *Phys. Rev. A* **77**, 054301 (2008), URL <https://link.aps.org/doi/10.1103/PhysRevA.77.054301>.
- [64] S. Das and G. S. Agarwal, *Journal of Physics B: Atomic, Molecular and Optical Physics* **42**, 205502 (2009).
- [65] R. Tanaś and Z. Ficek, *Physica Scripta* **2010**, 014037 (2010).

- [66] Z. Qiang, S. Ping, Z. Xiao-Ping, and R. Zhong-Zhou, *Communications in Theoretical Physics* **54**, 417 (2010).
- [67] V. S. Bhaskara and P. K. Panigrahi, *Quantum Information Processing* **16**, 118 (2017).
- [68] A. Nourmandipour, A. Vafafard, A. Morteza pour, and R. Franzosi, *Scientific Reports* **11**, 16259 (2021).
- [69] G. Vidal and R. F. Werner, *Phys. Rev. A* **65**, 032314 (2002), URL <https://link.aps.org/doi/10.1103/PhysRevA.65.032314>.
- [70] S. A. Hill and W. K. Wootters, *Phys. Rev. Lett.* **78**, 5022 (1997), URL <https://link.aps.org/doi/10.1103/PhysRevLett.78.5022>.
- [71] W. K. Wootters, *Phys. Rev. Lett.* **80**, 2245 (1998), URL <https://link.aps.org/doi/10.1103/PhysRevLett.80.2245>.
- [72] P. Rungta, V. Bužek, C. M. Caves, M. Hillery, and G. J. Milburn, *Phys. Rev. A* **64**, 042315 (2001), URL <https://link.aps.org/doi/10.1103/PhysRevA.64.042315>.
- [73] K. R. A. Hazzard, M. van den Worm, M. Foss-Feig, S. R. Manmana, E. G. Dalla Torre, T. Pfau, M. Kastner, and A. M. Rey, *Phys. Rev. A* **90**, 063622 (2014), URL <https://link.aps.org/doi/10.1103/PhysRevA.90.063622>.